Superconducting hydrogen tubes in hafnium hydrides at high pressure

Kun Gao,[1] Wenwen Cui,[1,*] Ju Chen,[1] Qinfang Wang,[1] Jian Hao,[1] Jingming Shi,[1] Cailong Liu,[2] Silvana Botti,[3,4] Miguel A. L. Marques,[5,4] and Yinwei Li[1,2,†]

[1]*Laboratory of Quantum Functional Materials Design and Application, School of Physics and Electronic Engineering, Jiangsu Normal University, Xuzhou 221116, China*

[2]*Shandong Key Laboratory of Optical Communication Science and Technology, School of Physical Science and Information Technology of Liaocheng University, Liaocheng 252059, China*

[3]*Institut für Festkörpertheorie und -optik, Friedrich-Schiller-Universität Jena, Max-Wien-Platz 1, 07743 Jena, Germany*

[4]*European Theoretical Spectroscopy Facility, Lund University, Box 118 221 00 Lund, Sweden*

[5]*Institut für Physik, Martin-Luther-Universität Halle-Wittenberg, D-06099 Halle, Germany*

(Received 28 February 2021; revised 8 July 2021; accepted 9 December 2021; published 27 December 2021)

Compressing hydrogen-rich hydrides is an effective method to search for exotic properties such as high-T_c superconductivity. Here we show that high pressure and high temperature stabilize unique hydrogen tubes in hafnium hydrides. A combination of structural searches and first-principle calculations predict a metastable stochiometric HfH_9 at 200 GPa. HfH_9 is composed of H tubes intercalated within Hf-H framework, where two-thirds of the hydrogen atoms are arranged in a tubelike H_{12} structure located inside channels formed by the remainder HfH_3. Each H_{12} tube gains 0.876 electrons from the HfH_3 framework, indicating the ionic character of HfH_9. Calculations show that HfH_9 is a potential superconductor with an estimated T_c of 110 K at 200 GPa, with the electron-phonon coupling arising mainly from the H_{12} tube and its interaction with the HfH_3 framework. The current results suggest the existence of diverse hydrogen chemistries at high pressure that could be unravelled by future experimental studies.

DOI: 10.1103/PhysRevB.104.214511

I. INTRODUCTION

The metallization of hydrogen has remained over the past decades a big challenge for experiments due to the extremely high pressure required, estimated above 500 GPa [1–4]. As an alternative, metallization could be achieved at much lower pressures in hydrogen-rich hydrides thanks to "chemical precompression" [5], making these hydrogen compounds the ideal test bed to study very high-temperature superconductivity [6–10]. This path has proved extremely successful, as evidenced by the recent theory-initiated discoveries of superconductivity at high temperature in H–S [11–13], LaH_{10} [14–18], and Y–H [19–22], and at room temperature in C-S-H [23–26].

Previous studies have demonstrated that high pressure is an effective method to stabilize superhydrides with the formation of new building blocks other than monoatomic H [27–31] and molecular H_2 [27,32–38]. Examples are linear or triangular H_3 [27,30,33,34,37,39–47], linear H_4 [27,48], pentagonal H_5 [6,49], H_8 cubes [50], penta-graphene-like H_{10} [6,16,49], honeycomb hydrogen layers [51–53], and H cages [14–21,28,48,54–63]. Among these, hydrides displaying H cages form a special class that exhibits extremely high-T_c superconductivity [14,16,19,28,56,59]. A sodalitelike H_{24} cage was first predicted in the high-pressure unconventional compound CaH_6, with an estimated T_c of 235 K at 150 GPa [28]. Thereafter, a theoretical study demonstrated that the compound YH_6 containing the same H_{24} cage was superconducting at temperatures as high as 260 K at 120 GPa [19], as confirmed by two recent experiments [20,21]. Further high-pressure stabilized hydrides accommodating diverse H cages were predicted to show high-T_c superconductivity: H_{29} cages in YH_9 [20] and CeH_9 [48,64] with T_c equal to 276 K (at 150 GPa) and 117 K (at 200 GPa), respectively; H_{32} cages in YH_{10} [14], LaH_{10} [14,15,18], and AcH_{10} [62] with T_c equal to 303 K (at 400 GPa), 274 K (at 250 GPa), and 251 K (at 200 GPa); H_{40} cages in AcH_{12} with 173 K (at 150 GPa); H_{24} cages in AcH_{16} [62] with 241 K (at 150 GPa); and coexisting H_{18} and H_{28} cages [56] in Li_2MgH_{16} with an astonishing T_c of 470 K (at 250 GPa). Interestingly, high-T_c superconductivity in CeH_9, CeH_{10} [65], CaH_6 [66,67], YH_9 [20,22], and LaH_{10} [15,17,18] has already been confirmed in experiments.

Besides hydrogen cages, the formation of other hydrogen units can lead to high-T_c superconductivity. For example, the T_c of SrH_6, that contains H_3 units, was predicted to be 156 K at 250 GPa, the highest found in H_3-structured hydrides [42]; the T_c of SnH_{12} with H_4 units [27], ScH_9 with H_5 units, and ScH_{10} with H_{10} units were estimated to be 93 K (at 250 GPa), 163 K (at 300 GPa), and 120 K (at 250 GPa) [49], respectively.

A recent study proposed that a metastable HfH_{10} with a penta-graphene-like H_{10} sublattice is superconducting below 234 K at 250 GPa [68]. In fact, previous studies demonstrated that high pressure could also stabilize several other superconducting Hf–H compounds in addition to the known HfH_2

*wenwencui@jsnu.edu.cn
†yinwei_li@jsnu.edu.cn

[69–75]. This includes the experimentally synthesized Hf_4H_{15} [76] and the theoretically predicted HfH, HfH_3, HfH_4, HfH_6, and HfH_{14} [7]. Very recently, HfH_6 with clathrate structure was proposed to become stable at 543 GPa, which possesses a maximum T_c of 132 K at 600 GPa [77].

Here, by performing a systematic structural search of the Hf–H binary system, we propose a superconducting HfH_9 that is dynamically stable at 200 GPa. Significantly, HfH_9 contains a hydrogen tube sublattice, which plays a key role in making this material superconducting below 110 K at 200 GPa.

II. COMPUTATIONAL DETAILS

The search for crystalline structures was performed using a particle-swarm optimization algorithm, as implemented in the CALYPSO code [78–80]. This method has been extremely successful in predicting stable and metastable superconducting hydrides [81], some of which have already been confirmed by experiments [11,14,16,19,23]. The predictions of the crystal structures of HfH_x (with $x = 1$–14) with up to four formula units were done from 0 to 200 GPa in intervals of 50 GPa. More than 2000 structures were sampled for each prediction run and the structural search can be well converged when ~1000 structures were generated after a lowest energy structure was found. Structural relaxations and electronic structure calculations were performed using the projector augmented-wave (PAW) method as implemented in the Vienna *Ab initio* Simulation Package (VASP) [82]. The exchange-correlation functional of density-functional theory was approximated by the generalized gradient approximation of Perdew, Burke, and Ernzerhof [83]. The all-electron PAW method was adopted for Hf and H atoms with valence $5p^6 6s^2 5d^2$, and $1s^1$, respectively. The cutoff energy for the expansion of the wave function in the plane wave basis was set to 1000 eV. Monkhorst-Pack k-point meshes [84] with a grid density of 0.20 $Å^{-1}$ were chosen to ensure a total energy convergence better than 1 meV per atom. The phonon spectrum and electron-phonon coupling were calculated within linear-response theory with the QUANTUM ESPRESSO code [85]. Ultrasoft pseudopotentials for Hf and H were used with a kinetic cutoff energy of 110 Ry [86]. First-principles molecular dynamics (MD) simulations [87] using the canonical NVT (N for the number of particles, V for volume, and T for temperature) were performed. The supercell $2 \times 2 \times 3$ (240 atoms) was used for $P6_3/m$ HfH_9. The canonical NVT ensemble uses a Nose-Hoover thermostat [88] with SMASS = 2 and each simulation consists of 16 000 time steps with a time step of 0.5 fs.

III. RESULTS AND DISCUSSION

Figure 1(a) depicts the formation enthalpy of the considered Hf–H compositions with respect to the decomposition to elementary substances at 200 GPa and 0 K with inclusion of zero-point energy (ZPE). Six thermodynamically stable hydrides with stoichiometries HfH, HfH_2, HfH_3, Hf_4H_{15}, HfH_4, and HfH_{14} (denoted by a filled symbol) form the vertices of the convex hull, consistent with previous results [68]. Furthermore, we find a series of other compounds that have formation enthalpies very close to the convex hull (at a distance of less than 10 meV/atom).

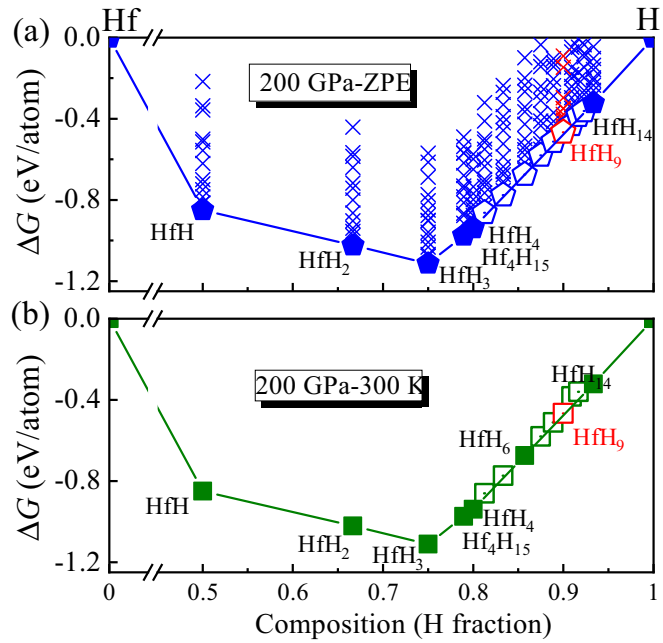

FIG. 1. Calculated Gibbs free energy (ΔG) of various Hf–H compounds with respect to the decomposition into Hf and H at 200 GPa and 0 K including the zero-point energy (ZPE) (a) and 300 K (b) denoted with pentagons and squares, respectively. The energetically stable phases are denoted by filled symbols connected with solid lines on the convex hull. The cross samples represent other metastable structures with higher energy for each stoichiometry without considering the ZPE effect. The inset is an enlarged view of area from HfH_6 to HfH_{14}.

It is well known that temperature is an effective means to alter the relative stability of competing phases, especially for hydrides due to the small mass of hydrogen. We therefore examined the effect of temperature on the formation energies of the Hf–H system using the quasiharmonic approximation. Figure 1(b) shows the convex hulls constructed at 300 K. We clearly see that another composition HfH_6 starts to lie on the convex hull. Note that HfH_6 was previously predicted to become energetically stable at pressures as high as 300 GPa at 0 K [68], suggesting that high temperature could effectively reduce the pressure needed to form these hydrides. The distance to the convex hull of HfH_9 at 0 K is about 10 meV/atom, which decreases to 8 meV/atom when temperature increased to 300 K within the quasiharmonic approximation. The following molecular dynamic simulations demonstrate that HfH_9 becomes diffusive at temperature above 300 K, preventing the estimation of the free energy based on quasiharmonic approximation. The decreased formation energy with increasing temperature suggests that HfH_9 could be synthesized at a much higher temperature, which could possibly persist at low temperature as a metastable structure. We performed *ab initio* molecular dynamic (AIMD) simulations at 150, 300, 500, and 1000 K to examine the stability of HfH_9 at 200 GPa. The calculated mean squared displacements (MSD) of the atomic positions and the configurations of the H and Hf atoms of the $P6_3/m$ phase of HfH_9 are shown in Fig. S1 of the Supplemental Material (SM) [89]. It is found that the HfH_9 remains solid

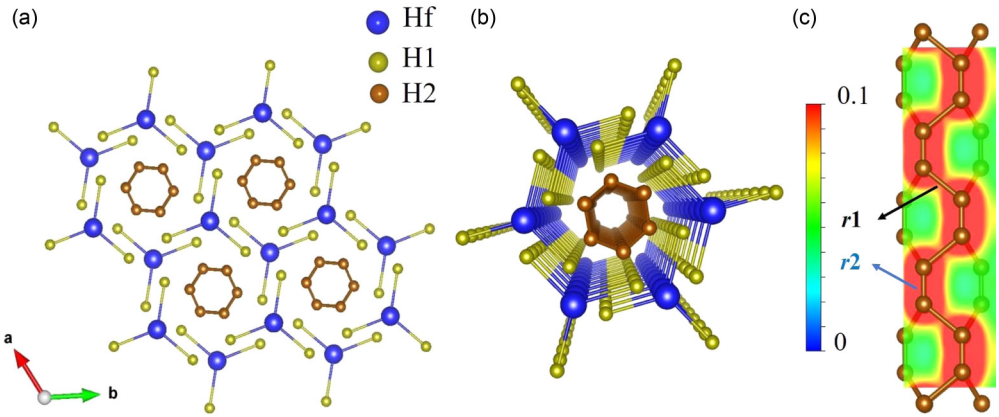

FIG. 2. (a) Crystal structure of $P6_3/m$-HfH_9 at 200 GPa, (b) the building block of HfH_9, (c) two-dimensional charge density (in units of e/bohr^3) of HfH_9 at 200 GPa. Blue, yellow, and brown spheres represent Hf and the two inequivalent hydrogen atoms, H1 and H2, respectively.

below 300 K without any diffuse for all the atoms (Figs. S1a and b), which means that there is a possibility that HfH_9 could persist at low temperature as a metastable structure once synthesized at high temperature. When the temperature increases to 500 K, the H atoms start to diffuse slightly (Fig. S1c), while the Hf-H framework can still be clearly observed. When the temperature further increases to 1000 K, HfH_9 transforms into a real superionic phase with fully diffusive H atoms inside the fixed Hf framework (Fig. S1d).

The HfH_9 phase has a hexagonal structure with space group $P6_3/m$ and two formula units per unit cell. The Hf atoms and two nonequivalent H1 and H2 atoms occupy the Wyckoff $2d$, $6h$, and $12i$ positions, respectively. As shown in Fig. 2(a), the $P6_3/m$ phase is composed of a hydrogen tube intercalated into a Hf–H1 framework, wherein each Hf atom is connected with three H1 atoms, forming planar HfH_3 units with a Hf–H1 bond distance of 1.76 Å. The HfH_3 units are then arranged such that they form hexagonal-like channels parallel to the c axis with a Hf $\cdots$ H1 distance of 1.81 Å. Interestingly, all 12 H2 atoms located inside the Hf–H1 channels form a tube structure (denoted as the H_{12} tube hereafter), clearly visible in Fig. 2(b). Notably, the H2 atoms are arranged in "H_2" molecules, leading to two different H–H distances: the intermolecular r_1 and intramolecular r_2 with bond lengths of 1.15 Å and 0.83 Å at 200 GPa, respectively [Fig. 2(c)]. The intramolecular H_2 bond length is slightly elongated as compared to the one in pure solid H_2 (0.74 Å), indicating the existence of strong interactions between these H_2 molecules. In fact, the length of r_1 is comparable to the H–H bonds in HfH_{10} (1.14 Å, at 200 GPa) [68], LaH_{10} (1.11 Å, at 200 GPa) [14], CsH_3 (1.24 Å, at 100 GPa) [43], NdH_9 (1.27 Å, at 120 GPa) [60], EuH_6 (1.3 Å, at 152 GPa) [55] and NaH_7 (1.25 Å, at 50 GPa) [41], and Li_2MgH_{16} (1.2 Å, at 300 GPa) [56], where the weak covalent nature of these bonds was already revealed.

To further examine the nature of the H–H bond in the H tubes, we calculated the integrated crystal orbital Hamiltonian population (ICOHP) [90] as shown in Fig. 3, where a more negative value hints at a stronger bond strength. At 200 GPa, the ICOHP for the intramolecular r_2 turns out to be -4.06 eV/pair, suggesting a strong covalent bond. As expected, the ICOHP for the intermolecular r_1 is only -1.12 eV/pair, which is comparable to the value of ~ -1 eV/pair (1.08 Å) for the H–H bond in the Li-Mg-H system [56], suggesting a comparative intermolecular interaction between the H_2 molecules, but much weaker than that of intramolecular covalent bonding interaction. The intermolecular interaction can also be seen by the localized electrons between the two hydrogen atoms [Fig. 2(c)]. Interestingly, the H_{12} tube is quite insensitive to pressure, in view of the nearly unchanged $r_1 = 1.11$ Å and $r_2 = 0.84$ Å, when pressure is increased to 250 GPa (Fig. S2 of the SM). This is understandable since the interaction between the Hf-H framework and H-tube structures is relatively weak, and the large space between them allows the HfH_3 framework to sustain almost the complete external compression. Indeed, the diameter of the Hf–H1 channel decreases

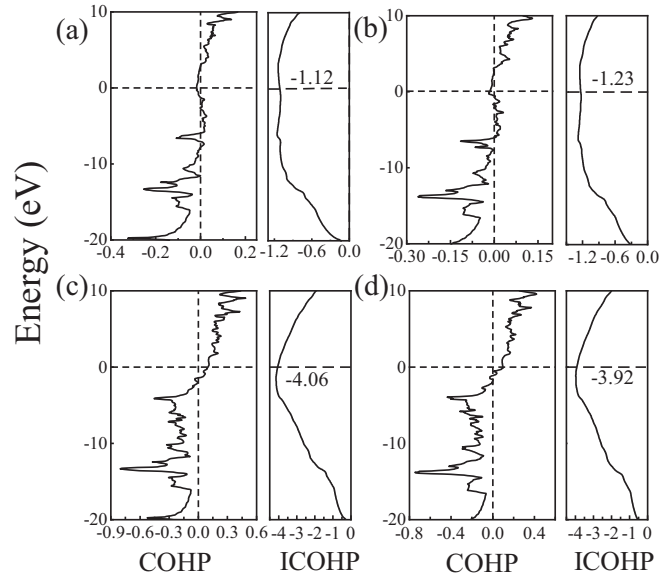

FIG. 3. Calculated crystalline orbital Hamiltonian population (COHP) and integrated crystalline orbital Hamiltonian population (ICOHP) of HfH_9 for H-H distances of inter-H-H distance (r_1) at 200 GPa (a) and 250 GPa (b). COHP and ICOHP for intra-H-H distance (r_2) at 200 GPa (c) and 250 GPa (d). The negative COHP indicates bonding and positive COHP indicates antibonding.

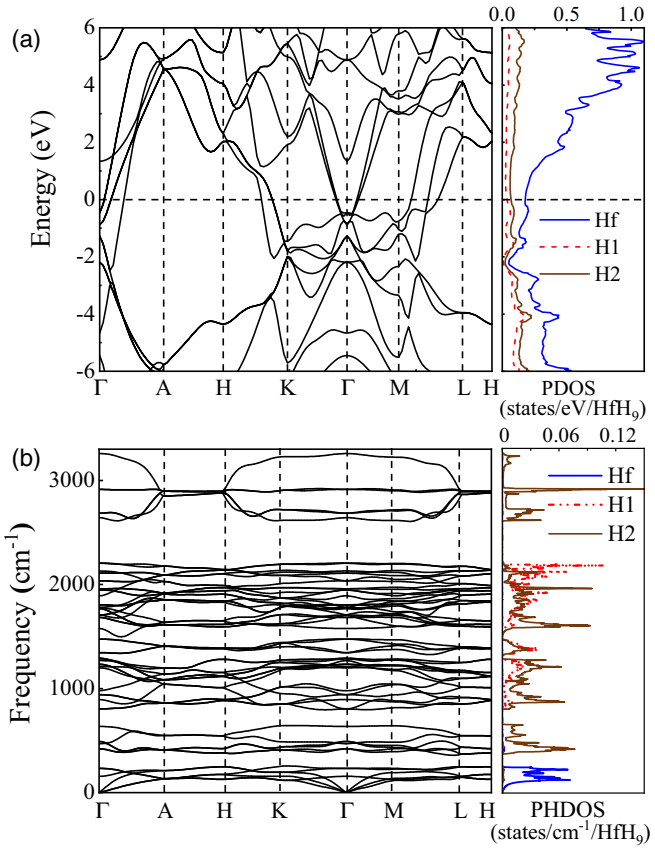

FIG. 4. (a) Electronic band structure and projected density of states (PDOS) and (b) phonon dispersion and projected phonon density of states (PHDOS) of HfH_9 at 200 GPa.

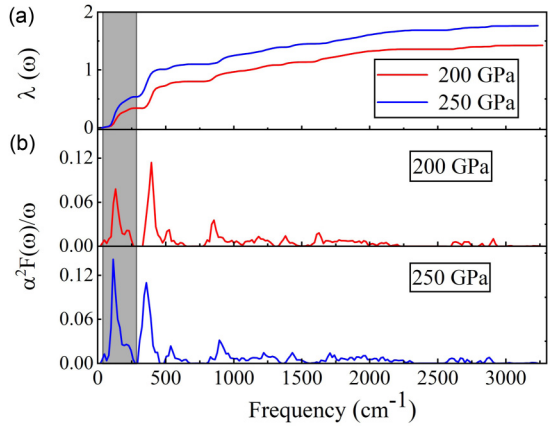

FIG. 5. (a) EPC constant $\lambda(\omega)$ and (b) Eliashberg spectral function $\alpha^2F(\omega)/\omega$ of HfH_9 at 200 and 250 GPa. The shaded region highlights the significant contribution of the first peak of $\alpha^2F(\omega)/\omega$ to λ.

from 4.45 Å at 200 GPa to 4.34 Å at 250 GPa. More interestingly, a Bader analysis [91] (Table SI of the SM) shows that each H_{12} tube in a unit cell receives 0.876*e* from the HfH_3 framework at 200 GPa, confirming the ionic nature of HfH_9.

We calculated the band structure and partial density of states (PDOS) of HfH_9 at 200 GPa to further explore its electronic properties [Fig. 4(a)]. HfH_9 exhibits a metallic behavior with several steep bands crossing the Fermi level. The total density of states at the Fermi level is 0.46 states/eV/f.u. at 200 GPa and increases to 0.5 states/eV/f.u. at 250 GPa (Fig. S3 of the SM). The PDOS shows a significant overlap of the contributions coming from Hf, H1, and H2 in a large energy range, indicating strong hybridization of Hf and H1 orbitals, as well as hybridization between the HfH_3 and the H_{12} tube. The phonon dispersion shown in Fig. 4(b) supports the dynamical stability of HfH_9 at 200 GPa in view of the absence of any imaginary frequencies. As expected, the frequencies below 250 cm^{-1} are distinctly dominated by Hf atoms due to their large mass, while the high end of the spectra is composed almost exclusively by the vibrations of the H atoms. Interestingly, the contribution from the H_{12} tube can be divided into three separated parts, two independent areas located around 500 cm^{-1} and 3000 cm^{-1}, respectively, and a hybrid area (790 cm^{-1}–2200 cm^{-1}) of vibrations involving both H1 and H2 atoms [see Fig. 4(b)].

In order to investigate the superconducting properties of HfH_9, we calculated the Eliashberg spectral function $\alpha^2F(\omega)/\omega$ and the integrated electron-phonon coupling (EPC) constant $\lambda(\omega)$ (see Fig. 5). The transition temperature T_c was then estimated from the spectral function by numerically solving the Eliashberg equations [92] with a typical choice of Coulomb pseudopotential $\mu^* = 0.1$. The resulting EPC parameter λ is 1.43 yielding a T_c of 110 K at 200 GPa. We found that vibrations of the hydrogen atoms contribute to 76% of the total λ, while the remainder comes from the low frequency Hf vibrations. Significantly, more than half of the contribution of H atoms comes from the hybrid frequency range, suggesting that the interaction between the HfH_3 and the H_{12} tube plays a key role in determining the high T_c of HfH_9. With the pressure increasing to 250 GPa, the total λ increases to 1.77, leading to a larger T_c of 130 K. The comparison of the Eliashberg spectral functions at the two pressures indicates that the increase of λ comes from the low frequency Hf vibrations, with a negligible contribution from the H_{12} tube, as highlighted by the gray area in Fig. 5. This is consistent with the previous analysis that high pressure has nearly no effect on the guest H_{12} tube. In this work, we neglected anharmonic effects, which tends to lower the T_c of hydrides [93–95], since this level of accuracy was beyond the scope of our exploratory work.

Further structural searches for HfH_9 are performed at 250 GPa and 300 GPa (Fig. S4). Phase transition occurs in HfH_9, from $P6_3/m$ phase to $C2/m$ at 270 GPa (Figs. S4a and b). We further calculated the Gibbs free energy of $C2/m$ with respect to HfH_6 and HfH_{14} from 0 K to 300 K at 300 GPa (Fig. S4c). The positive formation energy indicates that higher pressure or higher temperature are possibly needed in order to stabilize the HfH_9. Structure prediction runs were also performed at the lower pressures of 0–150 GPa, but no new stable stoichiometries were found (see Fig. S5 of the SM). Interestingly, we found that both HfH and HfH_4 remain energetically stable even at ambient pressure in addition to the previous known HfH_2 [69], as deduced from their location on the convex hull (Fig. S5). HfH has a tetragonal $P4_2/mmc$ structure at ambient pressure (Fig. S6a), which shows weak superconductivity with an estimated T_c of 0.35 K. The low T_c

in HfH is reasonable if we consider the negligible contribution of H to the total DOS at the Fermi level (Fig. S7a). The structure of HfH_4 at ambient pressure has orthorhombic $Pna2_1$ symmetry (Fig. S6b), and is a semiconductor with a band gap of 0.4 eV (Fig. S7b). Additionally, the structures and electronic properties of other dynamically stable compounds with formation enthalpy close to the convex HfH_x ($x = 5, 7, 8$) (see Figs. S6– S8 and Table SII) are also provided in the SM as references for future experimental study.

IV. CONCLUSIONS

In summary, our combination of structure prediction and first-principle calculations has predicted a metastable HfH_9 compound at 200 GPa. HfH_9 contains a unique H_{12}-tube structure that is located inside channels formed by the remaining HfH_3 sublattice. Phonon calculations indicate that HfH_9 is dynamically stable as the temperature was cooled down to 0 K. Interestingly, HfH_9 appears to be superconducting with an estimated T_c of 110 K at 200 GPa, mainly due to the interaction between the H_{12} tube and the HfH_3 sublattice. Our findings suggest that the combination of high pressure is an effective path to form superhydrides as well as hydrogen structures exhibiting exotic properties.

ACKNOWLEDGMENTS

The authors acknowledge funding from the NSFC under Grants No. 12074154, No. 11722433, No. 11804128, and No. 11804129. W.C. and M.A.L.M. acknowledge the funding from the Sino-German Mobility Programme under Grant No. M-0362. Y.L. acknowledges the funding from the Six Talent Peaks Project and 333 High-level Talents Project of Jiangsu Province. K.G. acknowledges the funding from Postgraduate Research & Practice Innovation Program of Jiangsu Province No. KYCX20_2216. J.H. acknowledges the funding from the Science and Technology Project of Xuzhou under Grant No. KC19010. All the calculations were performed at the High Performance Computing Center of the School of Physics and Electronic Engineering of Jiangsu Normal University.

[1] E. Wigner and H. B. Huntington, J. Chem. Phys. **3**, 764 (1935).
[2] S. Azadi, B. Monserrat, W. M. C. Foulkes, and R. J. Needs, Phys. Rev. Lett. **112**, 165501 (2014).
[3] T. Bi, N. Zarifi, T. Terpstra, and E. Zurek, The search for superconductivity in high pressure hydrides, in *Reference Module in Chemistry, Molecular Sciences and Chemical Engineering*, edited by J. Reedijk (Elsevier, 2019), pp. 1–36.
[4] J. McMinis, R. C. Clay III, D. Lee, and M. A. Morales, Phys. Rev. Lett. **114**, 105305 (2015).
[5] N. W. Ashcroft, Phys. Rev. Lett. **92**, 187002 (2004).
[6] E. Zurek and T. Bi, J. Chem. Phys. **150**, 050901 (2019).
[7] D. V. Semenok, I. A. Kruglov, I. A. Savkin, A. G. Kvashnin, and A. R. Oganov, Curr. Opin. Solid State Mater. Sci. **24**, 100808 (2020).
[8] J. A. Flores-Livas, L. Boeri, A. Sanna, G. Profeta, R. Arita, and M. Eremets, Phys. Rep. **856**, 1 (2020).
[9] H. Wang, X. Li, G. Gao, Y. Li, and Y. Ma, WIREs Comput. Mol. Sci. **8**, e1330 (2018).
[10] J. Lv, Y. Sun, H. Liu, and Y. Ma, Matter Radiat. Extremes **5**, 068101 (2020).
[11] Y. Li, J. Hao, H. Liu, Y. Li, and Y. Ma, J. Chem. Phys. **140**, 174712 (2014).
[12] D. Duan, Y. Liu, F. Tian, D. Li, X. Huang, Z. Zhao, H. Yu, B. Liu, W. Tian, and T. Cui, Sci. Rep. **4**, 6968 (2014).
[13] A. Drozdov, M. Eremets, I. Troyan, V. Ksenofontov, and S. I. Shylin, Nature (London) **525**, 73 (2015).
[14] H. Liu, I. I. Naumov, R. Hoffmann, N. Ashcroft, and R. J. Hemley, Proc. Natl. Acad. Sci. USA **114**, 6990 (2017).
[15] M. Kostrzewa, K. Szczśniak, A. Durajski, and R. Szczśniak, Sci. Rep. **10**, 1592 (2020).
[16] F. Peng, Y. Sun, C. J. Pickard, R. J. Needs, Q. Wu, and Y. Ma, Phys. Rev. Lett. **119**, 107001 (2017).
[17] A. Drozdov, P. Kong, V. Minkov, S. Besedin, M. Kuzovnikov, S. Mozaffari, L. Balicas, F. Balakirev, D. Graf, V. Prakapenka *et al.*, Nature (London) **569**, 528 (2019).
[18] M. Somayazulu, M. Ahart, A. K. Mishra, Z. M. Geballe, M. Baldini, Y. Meng, V. V. Struzhkin, and R. J. Hemley, Phys. Rev. Lett. **122**, 027001 (2019).
[19] Y. Li, J. Hao, H. Liu, S. T. John, Y. Wang, and Y. Ma, Sci. Rep. **5**, 9948 (2015).
[20] P. Kong, V. Minkov, M. Kuzovnikov, A. Drozdov, S. Besedin, S. Mozaffari, L. Balicas, F. Balakirev, V. Prakapenka, S. Chariton *et al.*, Nat. Commun. **12**, 5075 (2021).
[21] I. A. Troyan, D. V. Semenok, A. G. Kvashnin, A. V. Sadakov, O. A. Sobolevskiy, V. M. Pudalov, A. G. Ivanova, V. B. Prakapenka, E. Greenberg, A. G. Gavriliuk *et al.*, Adv. Mater. **33**, 2006832 (2021).
[22] E. Snider, N. Dasenbrock-Gammon, R. McBride, X. Wang, N. Meyers, K. V. Lawler, E. Zurek, A. Salamat, and R. P. Dias, Phys. Rev. Lett. **126**, 117003 (2021).
[23] W. Cui, T. Bi, J. Shi, Y. Li, H. Liu, E. Zurek, and R. J. Hemley, Phys. Rev. B **101**, 134504 (2020).
[24] Y. Sun, Y. Tian, B. Jiang, X. Li, H. Li, T. Iitaka, X. Zhong, and Y. Xie, Phys. Rev. B **101**, 174102 (2020).
[25] E. Snider, N. Dasenbrock-Gammon, R. McBride, M. Debessai, H. Vindana, K. Vencatasamy, K. V. Lawler, A. Salamat, and R. P. Dias, Nature (London) **586**, 373 (2020).
[26] S. Hu, R. Paul, V. Karasiev, and R. Dias, arXiv:2012.10259.
[27] M. M. D. Esfahani, Z. Wang, A. R. Oganov, H. Dong, Q. Zhu, S. Wang, M. S. Rakitin, and X.-F. Zhou, Sci. Rep. **6**, 22873 (2016).
[28] H. Wang, S. T. John, K. Tanaka, T. Iitaka, and Y. Ma, Proc. Natl. Acad. Sci. USA **109**, 6463 (2012).
[29] D. Y. Kim, R. H. Scheicher, and R. Ahuja, Phys. Rev. B **78**, 100102(R) (2008).
[30] D. Zhou, X. Jin, X. Meng, G. Bao, Y. Ma, B. Liu, and T. Cui, Phys. Rev. B **86**, 014118 (2012).
[31] J. Zhang, J. M. McMahon, A. R. Oganov, X. Li, X. Dong, H. Dong, and S. Wang, Phys. Rev. B **101**, 134108 (2020).
[32] A. Shamp and E. Zurek, Novel Supercond. Mater. **3**, 14 (2017).

[33] W. Chen, D. V. Semenok, A. G. Kvashnin, X. Huang, I. A. Kruglov, M. Galasso, H. Song, D. Duan, A. F. Goncharov, V. B. Prakapenka *et al.*, Nat. Commun. **12**, 273 (2021).

[34] X. Zhong, H. Wang, J. Zhang, H. Liu, S. Zhang, H.-F. Song, G. Yang, L. Zhang, and Y. Ma, Phys. Rev. Lett. **116**, 057002 (2016).

[35] T. A. Strobel, M. Somayazulu, and R. J. Hemley, Phys. Rev. Lett. **103**, 065701 (2009).

[36] G. Gao, A. R. Oganov, A. Bergara, M. Martinez-Canales, T. Cui, T. Iitaka, Y. Ma, and G. Zou, Phys. Rev. Lett. **101**, 107002 (2008).

[37] D. Duan, Y. Liu, Y. Ma, Z. Shao, B. Liu, and T. Cui, Natl. Sci. Rev. **4**, 121 (2017).

[38] E. Zurek, R. Hoffmann, N. Ashcroft, A. R. Oganov, and A. O. Lyakhov, Proc. Natl. Acad. Sci. USA **106**, 17640 (2009).

[39] E. Zurek, Comments Inorg. Chem. **37**, 78 (2017).

[40] J. Hooper and E. Zurek, Chem. - Eur. J. **18**, 5013 (2012).

[41] V. V. Struzhkin, D. Y. Kim, E. Stavrou, T. Muramatsu, H.-k. Mao, C. J. Pickard, R. J. Needs, V. B. Prakapenka, and A. F. Goncharov, Nat. Commun **7**, 12267 (2016).

[42] Y. Wang, H. Wang, S. T. John, T. Iitaka, and Y. Ma, Phys. Chem. Chem. Phys. **17**, 19379 (2015).

[43] A. Shamp, J. Hooper, and E. Zurek, Inorg. Chem. **51**, 9333 (2012).

[44] J. Hooper, B. Altintas, A. Shamp, and E. Zurek, J. Phys. Chem. C **117**, 2982 (2013).

[45] D. Duan, X. Huang, F. Tian, Y. Liu, D. Li, H. Yu, B. Liu, W. Tian, and T. Cui, J. Phys. Chem. A **119**, 11059 (2015).

[46] Y. Liu, D. Duan, F. Tian, H. Liu, C. Wang, X. Huang, D. Li, Y. Ma, B. Liu, and T. Cui, Inorg. Chem. **54**, 9924 (2015).

[47] Z. Wang, H. Wang, S. T. John, T. Iitaka, and Y. Ma, Chem. Sci. **6**, 522 (2015).

[48] N. P. Salke, M. M. D. Esfahani, Y. Zhang, I. A. Kruglov, J. Zhou, Y. Wang, E. Greenberg, V. B. Prakapenka, J. Liu, A. R. Oganov *et al.*, Nat. Commun. **10**, 4453 (2019).

[49] X. Ye, N. Zarifi, E. Zurek, R. Hoffmann, and N. Ashcroft, J. Phys. Chem. C **122**, 6298 (2018).

[50] I. A. Kruglov, A. G. Kvashnin, A. F. Goncharov, A. R. Oganov, S. S. Lobanov, N. Holtgrewe, S. Jiang, V. B. Prakapenka, E. Greenberg, and A. V. Yanilkin, Sci. Adv. **4**, eaat9776 (2018).

[51] A. G. Kvashnin, I. A. Kruglov, D. V. Semenok, and A. R. Oganov, J. Phys. Chem. C **122**, 4731 (2018).

[52] A. Majumdar, J. S. Tse, M. Wu, and Y. Yao, Phys. Rev. B **96**, 201107(R) (2017).

[53] C. Pépin, G. Geneste, A. Dewaele, M. Mezouar, and P. Loubeyre, Science **357**, 382 (2017).

[54] D. V. Semenok, D. Zhou, A. G. Kvashnin, X. Huang, M. Galasso, I. A. Kruglov, A. G. Ivanova, A. G. Gavriliuk, W. Chen, N. V. Tkachenko *et al.*, J. Phys. Chem. Lett. **12**, 32 (2020).

[55] L. Ma, M. Zhou, Y. Wang, S. Kawaguchi, Y. Ohishi, F. Peng, H. Liu, G. Liu, H. Wang, and Y. Ma, Phys. Rev. Research **3**, 043107 (2021).

[56] Y. Sun, J. Lv, Y. Xie, H. Liu, and Y. Ma, Phys. Rev. Lett. **123**, 097001 (2019).

[57] W. Sun, X. Kuang, H. D. J. Keen, C. Lu, and A. Hermann, Phys. Rev. B **102**, 144524 (2020).

[58] M. Peña-Alvarez, J. Binns, A. Hermann, L. C. Kelsall, P. Dalladay-Simpson, E. Gregoryanz, and R. T. Howie, Phys. Rev. B **100**, 184109 (2019).

[59] D. V. Semenok, A. G. Kvashnin, A. G. Ivanova, V. Svitlyk, V. Y. Fominski, A. V. Sadakov, O. A. Sobolevskiy, V. M. Pudalov, I. A. Troyan, and A. R. Oganov, Mater. Today **33**, 36 (2020).

[60] D. Zhou, D. V. Semenok, H. Xie, X. Huang, D. Duan, A. Aperis, P. M. Oppeneer, M. Galasso, A. I. Kartsev, A. G. Kvashnin *et al.*, J. Am. Chem. Soc. **142**, 2803 (2020).

[61] D. Zhou, D. V. Semenok, D. Duan, H. Xie, W. Chen, X. Huang, X. Li, B. Liu, A. R. Oganov, and T. Cui, Sci. Adv. **6**, eaax6849 (2020).

[62] D. V. Semenok, A. G. Kvashnin, I. A. Kruglov, and A. R. Oganov, J. Phys. Chem. Lett. **9**, 1920 (2018).

[63] H. Song, Z. Zhang, T. Cui, C. J. Pickard, V. Z. Kresin, and D. Duan, Chinese Phys. Lett. **38**, 107401 (2021).

[64] X. Li, X. Huang, D. Duan, C. J. Pickard, D. Zhou, H. Xie, Q. Zhuang, Y. Huang, Q. Zhou, B. Liu *et al.*, Nat. Commun. **10**, 3461 (2019).

[65] W. Chen, D. V. Semenok, X. Huang, H. Shu, X. Li, D. Duan, T. Cui, and A. R. Oganov, Phys. Rev. Lett. **127**, 117001 (2021).

[66] L. Ma, K. Wang, Y. Xie, X. Yang, Y. Wang, M. Zhou, H. Liu, G. Liu, H. Wang, and Y. Ma, arXiv:2103.16282.

[67] Z. Li, X. He, C. Zhang, S. Zhang, S. Feng, X. Wang, R. Yu, and C. Jin, arXiv:2103.16917.

[68] H. Xie, Y. Yao, X. Feng, D. Duan, H. Song, Z. Zhang, S. Jiang, S. A. T. Redfern, V. Z. Kresin, C. J. Pickard, and T. Cui, Phys. Rev. Lett. **125**, 217001 (2020).

[69] Y. Liu, X. Huang, D. Duan, F. Tian, H. Liu, D. Li, Z. Zhao, X. Sha, H. Yu, H. Zhang *et al.*, Sci. Rep. **5**, 11381 (2015).

[70] S. Sidhu and J. McGuire, J. Appl. Phys. **23**, 1257 (1952).

[71] N. Bourgeois, J.-C. Crivello, P. Cenedese, and J.-M. Joubert, ACS Comb. Sci. **19**, 513 (2017).

[72] D. Papaconstantopoulos and A. Switendick, J. Less-Common Met. **103**, 317 (1984).

[73] R. Quijano, R. de Coss, and D. J. Singh, Phys. Rev. B **80**, 184103 (2009).

[74] R. S. Gupta and S. Chatterjee, J. Phys. F: Met. Phys. **14**, 631 (1984).

[75] S. Sidhu, L. Heaton, and D. Zauberis, Acta Crystallogr. **9**, 607 (1956).

[76] M. A. Kuzovnikov and M. Tkacz, J. Phys. Chem. C **123**, 30059 (2019).

[77] P. Tsuppayakorn-Aek, N. Phaisangittisakul, R. Ahuja, and T. Bovornratanaraks, Sci. Rep. **11**, 16403 (2021).

[78] Y. Wang, J. Lv, L. Zhu, and Y. Ma, Phys. Rev. B **82**, 094116 (2010).

[79] Y. Wang, J. Lv, L. Zhu, and Y. Ma, Comput. Phys. Commun. **183**, 2063 (2012).

[80] B. Gao, P. Gao, S. Lu, J. Lv, Y. Wang, and Y. Ma, Sci. Bull. **64**, 301 (2019).

[81] W. Cui and Y. Li, Chin. Phys. B **28**, 107104 (2019).

[82] G. Kresse and J. Furthmüller, Phys. Rev. B **54**, 11169 (1996).

[83] J. P. Perdew, K. Burke, and M. Ernzerhof, Phys. Rev. Lett. **77**, 3865 (1996).

[84] W. Tang, E. Sanville, and G. Henkelman, J. Phys.: Condens. Matter **21**, 084204 (2009).
[85] P. Giannozzi, S. Baroni, N. Bonini, M. Calandra, R. Car, C. Cavazzoni, D. Ceresoli, G. L. Chiarotti, M. Cococcioni, I. Dabo *et al.*, J. Phys.: Condens. Matter **21**, 395502 (2009).
[86] G. Kresse and D. Joubert, Phys. Rev. B **59**, 1758 (1999).
[87] S. Nosé, J. Chem. Phys. **81**, 511 (1984).
[88] W. G. Hoover, Phys. Rev. A **31**, 1695 (1985).
[89] See Supplemental Material at http://link.aps.org/supplemental/10.1103/PhysRevB.104.214511. It contains the charges' transfer, the electronic properties and phonon dispersions of other compounds at different pressure and structure information of all the compounds, etc.
[90] R. Dronskowski and P. E. Blöchl, J. Phys. Chem. **97**, 8617 (1993).
[91] G. Henkelman, A. Arnaldsson, and H. Jónsson, Comput. Mater. Sci. **36**, 354 (2006).
[92] G. Eliashberg, Sov. Phys. JETP **11**, 696 (1960).
[93] I. Errea, M. Calandra, C. J. Pickard, J. Nelson, R. J. Needs, Y. Li, H. Liu, Y. Zhang, Y. Ma, and F. Mauri, Phys. Rev. Lett. **114**, 157004 (2015).
[94] I. Errea, F. Belli, L. Monacelli, A. Sanna, T. Koretsune, T. Tadano, R. Bianco, M. Calandra, R. Arita, F. Mauri *et al.*, Nature (London) **578**, 66 (2020).
[95] P. Hou, F. Belli, R. Bianco, and I. Errea, Phys. Rev. B **103**, 134305 (2021).